fluids

MDPI

Review

A Short Review on the Rheology of Twist Grain Boundary-A and Blue Phase Liquid Crystals

Rasmita Sahoo and Surajit Dhara *

School of Physics, University of Hyderabad, Hyderabad 500046, India; rasmita.phy@gmail.com
* Correspondence: sdsp@uohyd.ernet.in

Received: 22 February 2018; Accepted: 4 April 2018; Published: 9 April 2018

Abstract: Topological defects are important in determining the properties of physical systems and are known varyingly depending on the broken symmetry. In superfluid helium, they are called vortices; in periodic crystals, one refers to dislocations; and in liquid crystals, they are disclinations. The defects and the inter-defect interaction in some highly chiral liquid crystals stabilize some intermediate complex phases such as Blue Phases (BPs) and Twist Grain Boundary-A (TGB_A) phases. The defect dynamics of these phases contributes to the rheological properties. The temperature range of these intermediate phases usually are very small in pure liquid crystals; consequently, a detailed experiment has been difficult to achieve. However, the temperature range could be enhanced significantly in multicomponent systems. In this review article, we discuss some recent experimental progress made in understanding the rheological properties of the wide-temperature-range TGB_A and BP liquid crystals.

Keywords: liquid crystals; topological defects; TGB_A; BPs; rheology

1. Introduction

Liquid crystals belong to the broad class of soft matter, which appears in between crystalline solids and isotropic liquids. They are usually made of shape anisotropic organic molecules and exhibit a variety of phase transitions. A nematic is one of the simplest liquid crystals in which the constituent molecules have a preference to align with one another along one orientation in the system called the director and denoted by a dimensionless unit vector $\hat{n}$. The nematic is apolar, i.e., $\hat{n}$ and $-\hat{n}$ are physically equivalent. In the nematic phase, two different types of topological defects or singularities are observed. These are either line defects, known as disclinations (showing the discontinuity in the inclination of molecules) or point defects (hedgehogs and boojums) where the director cannot be defined [1,2]. These defects cannot be eliminated by continuous deformation of the order parameter field; hence, they are topologically stable [3]. They are characterized by strength or winding number 's', which is denoted by an integer or half-integer number. The strength 's' determines the number of times the director rotates around the singularity when one encircles the defect core [2]. Two oppositely-charged defects can annihilate one other. The orientation of the nematic director field (ψ) surrounding the defect can be expressed in terms of defect strength (s) [1]:

$$\psi = s\alpha + \beta \tag{1}$$

where $\alpha = \tan^{-1}(y/x)$ and β is a constant. Here, the defect strength s depends on the symmetry of the medium. In the nematic phase, s is the multiple of $\pm\frac{1}{2}$, as the director has $\hat{n} \equiv -\hat{n}$ symmetry. Figure 1 shows the schematic representation of the director structure of a few defects.

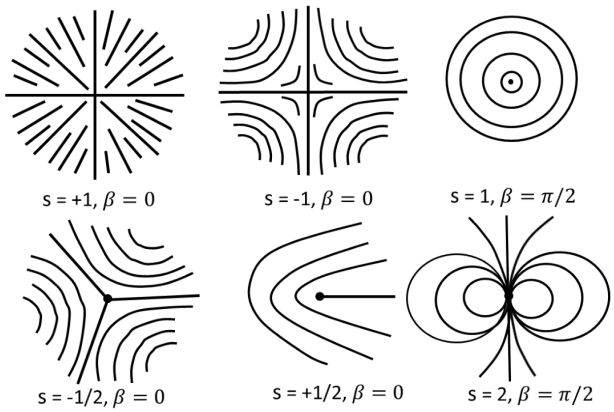

Figure 1. Schematic representation of a few defects with different winding numbers. Continuous lines represent the director field around the singularity.

In the cholesteric phase (N^*), the molecular chirality induces spontaneous twist, which leads to complicated, but stable networks of disclination lines in a planar cell, known as oily-streak defects [4]. These defects are easily observed under a polarizing optical microscope (POM). Smectic liquid crystals exhibit dislocations due to the layered structure. In this case, the distortion alters the smectic layer displacement field u, which leads to the dislocations in the medium and is defined as [3]:

$$\oint_{\Gamma} d\mathbf{u} = (kd)\hat{z} = \mathbf{b} \tag{2}$$

where $\hat{z}$ signifies the direction of the lattice distortion, d is the layer spacing and **b** is called Burger's vector. Here, the nature of the defects depends on the relative orientations of **b** and the dislocation line. A schematic representation of dislocations in the SmA phase is shown in Figure 2. If **b** is parallel to the dislocation line, it is called the "screw dislocations" (Figure 2a). The smectic layers climb up or down by an integral number of d upon going round the dislocation line, changing in a screw-like manner. On the other hand, if **b** is perpendicular to the dislocation line, it is called an "edge dislocation" (Figure 2b). In this case, a few layers are either added or removed from one side of the dislocation line. The dislocation lines cannot be observed under POM. In addition to dislocations, smectic liquid crystals also show focal conic defects, and these defects can be observed under POM [2].

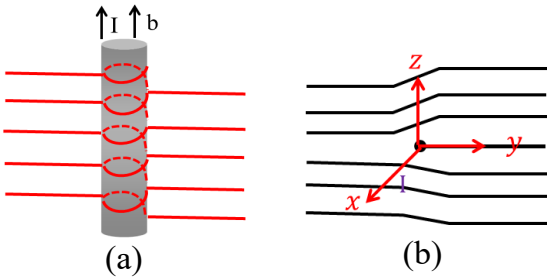

Figure 2. (Color online) (**a**) Schematic representation of screw dislocations in the SmA phase. The cross-section shown here indicates that each layer changes height by half a layer in half a circuit of the defect core. The dislocation line is denoted by I, parallel to Burger's vector and $b = +d$. (**b**) An edge dislocation with $b = -d$.

1.1. Twist Grain Boundary Phase

In highly chiral liquid crystals in between the cholesteric and SmA phase, occasionally, an intermediate phase with a relatively larger pitch is observed. In smectics, when molecular chirality

increases, the competition between the twist formation and smectic layer formation leads to some frustrated structures, known as twist grain boundary phases [5]. This is a thermodynamically-stable phase. Experimentally, it was first observed by Goodby et al. [6]. The Twist Grain Boundary-A (TGB_A) phase has an analogy with the Abrikosov phase of Type-II superconductors in an external magnetic field, and it was first proposed by de Gennes [1,5]. Hence, they are also called Type-II smectic liquid crystals. In this analogy, the twist of a cholesteric phase penetrates into the SmA structure through a lattice of screw dislocations, which is similar to the magnetic flux lines penetrating a Type-II superconductor via a lattice of vortices. The detailed structure was theoretically calculated by Renn and Lubensky [5]. A schematic representation of the arrangement of smectic-A blocks of the TGB_A phase is shown in Figure 3. The parallel screw dislocations originate due to the rotation of successive smectic slabs relative to each other. The well-defined SmA blocks are separated by regularly-spaced planar arrays of parallel screw dislocations. The interaction between the dislocations forms grain boundaries, and the interaction among the grain boundaries stabilizes the TGB_A structure. The typical distance between two dislocations in a grain boundary is denoted as l_d, and the inter-grain boundary distance as l_b and usually $l_d \sim l_b$, and they are in the range of 20–30 nm [7]. Later, several variants of the twist grain boundary phase were observed such as TGB_C [8], TGB_{C^*} [9], $UTGB_{C^*}$ [10,11], etc. $UTGB_{C^*}$ has a three-dimensionally-modulated structure, and it was discovered in a binary mixture of a chiral and a nonchiral compounds.

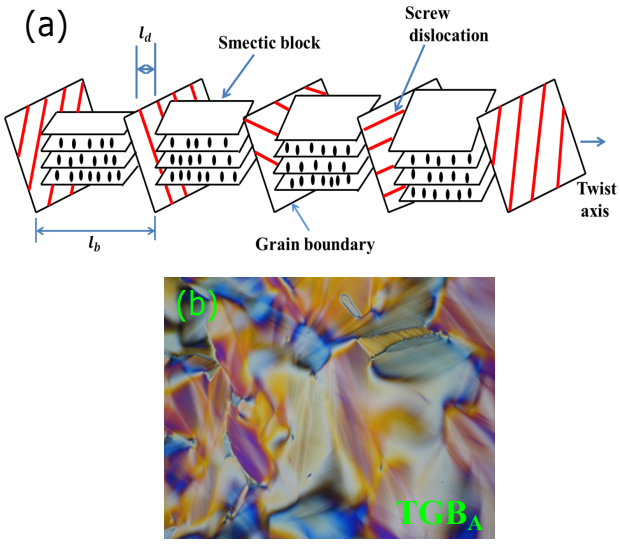

Figure 3. (Color online) (**a**) Schematic diagram showing the structure of the Twist Grain Boundary-A (TGB_A) phase. The distance between two dislocations and two grain boundaries are l_d and l_b respectively. (**b**) A typical texture of the TGB_A phase with relatively large pitch in the planar surface anchoring condition. The different colors indicate the different twist regions formed during cooling from the N^* phase. Reproduced with permission from [12].

1.2. Blue Phases

Blue phases are another type of frustrated phase observed in highly chiral liquid crystals. They appear between the Isotropic (I) and cholesteric (N^*) phase transition, and the temperature range in pure compounds is very narrow (~1 K). In the early investigations, they appeared blue, hence being known as the blue phase. The defect-lattice structure and POM textures of BP-I and BP-II are shown in Figure 4. In the cholesteric phase, the orientation of the local director can twist around two perpendicular axes, and the corresponding deformed structure is named as a "double-twist cylinder" [1]. The double twist cylinders fill up the volume by stabilizing a lattice of defect-disclinations [13,14]. The defect lines arrange themselves forming different structures,

and depending on their local arrangement, they are classified into Blue Phase (BP)-I, BP-II and BP-III. The BP-I, BP-II and BP-III have body-centered cubic, simple cubic and amorphous structure, respectively. The symmetry of BP-III is almost similar to the isotropic phase, hence it is very difficult to distinguish from the isotropic phase under POM. BP-I and BP-II can be identified under POM rather easily. The stability of BP-I increases with increasing chirality, whereas BP-II prevails up to a certain range of the temperature-chirality variation. There are a few methods known to increase the temperature range of BPs such as by dispersion of the polymer, nanoparticles and mixing of many liquid crystals and chiral dopant. Among them, polymer-stabilized BPs are very popular, and they were discovered by Kikuchi et al. [15]. They showed that the range can be enhanced to more than 60 K and down to room temperature. This created immense interest in the field of liquid crystals, and consequently polymer-stabilized liquid crystal displays (LCDs) with superior display performance were reported [16–19]. There are many studies that have reported on the complex structure and optical properties of blue phases. Nevertheless, several fundamental aspects of these exotic phases are yet to be explored. For example, recently, several theoretical predictions were made on the defect dynamics and rheological properties of BP-II and BP-I [20–24], which are yet to be explored experimentally.

2. Experimental Section

Most of the rheological measurements, unless specifically mentioned, reported here were performed by a controlled strain Rheometer (MCR 501, Anton Paar, Graz, Austria) with cone-plate or parallel plate measuring systems. A Peltier temperature controller with an accuracy of 0.1 °C was used to vary the temperature. All the measurements were made on cooling the sample from the isotropic phase. The samples were presheared at the shear rate of 10 s^{-1} for 400 s before starting the measurements. The details of the rheomicroscopy setup are given in [25,26].

3. Rheological Properties of the Twist Grain Boundary-A Phase

In pure compounds, the temperature range of the TGB_A phase is usually very short (1–2 °C). Nevertheless, some attempts were made to characterize the rheological properties. Asnacios et al. studied the rheological properties of Cholesteryl Tetradecanoate (CT) and Cholesteryl Nonanoate (CN) and focused on the rheological properties near the N^*-SmA transition [27]. From the temperature-dependent viscosity and shear rate-dependent shear stress, they found a short-range smectic-like behavior just above the SmA-N^* transition ($T = T_{N^*\text{-SmA}} + 1$ °C). They conjectured it to be a TGB-like phase. Later, Rajeswari et al. also studied the rheological properties of CN and its mixture with 4′-octyloxy-4-cyanobiphenyl (8OCB) [12]. They confirmed that indeed, a short-range smectic-like order in the cholesteric phase exists, and it was further enhanced by mixing a small amount of 8OCB compound. Figure 5 shows the temperature-dependent shear viscosity of the mixture with 20 wt % 8OCB. Apart from a sharp peak in the viscosity due to the blue phases, they observed another anomalous peak across the N^*-SmA transition. The latter one was attributed to the SmA to TGB_A phase transition. However, the narrow temperature range has always been a major problem to understand and correlate its physical properties with the structure.

Recently, Rasmita et al. studied the rheological properties of a TGB_A phase with a wide temperature-range [25]. It was discovered in a binary mixture of two compounds, namely 4-(2′-methyl butyl phenyl)4′-n-octylbiphenyl-4-carboxylate (CE8) and 2-cyano-4-heptyl-phenyl-4′-pentyl-4-biphenyl carboxylate (7(CN)5), where CE8 is a chiral and 7(CN)5 is a nonchiral compound, by Pramod et al. [10,11]. Sixty-three-point-six weight percent of CE8 and 36.4 wt % of 7(CN)5 in the mixture are known to show the following phase transitions: I 123 °C N^* 83.5 °C TGB_A 60.2 °C SmC *. Thus, the temperature range of the TGB_A phase is about 20 °C. The phase transitions were identified from the temperature-dependent shear viscosity measurements (Figure 6). The shear viscosity of the TGB_A phase is two orders of magnitude larger than that of the cholesteric phase.

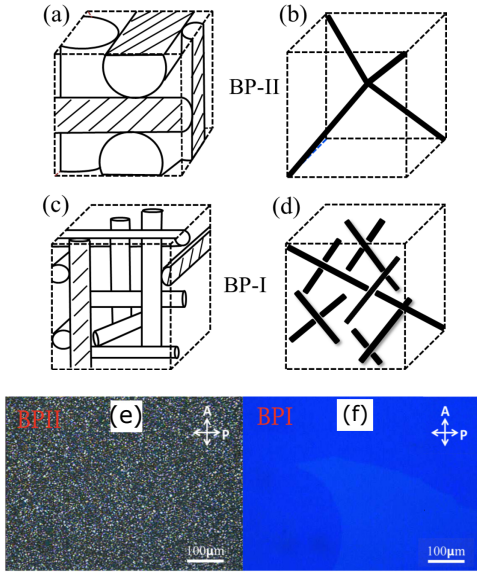

Figure 4. Schematic diagrams of the BP-II and BP-I. (**a**,**c**) Spatial arrangements of double twisted cylinders in unit cells; (**b**) simple cubic unit cell of the disinclination lattice in BP-II; (**d**) body-centered cubic unit cell of the disinclination lattice in BP-I; the black lines in (**b**,**d**) are the defect-disinclinations; (**e**,**f**) typical textures of BP-II and BP-I observed under a polarizing optical microscope (POM). Reproduced with permission from [26].

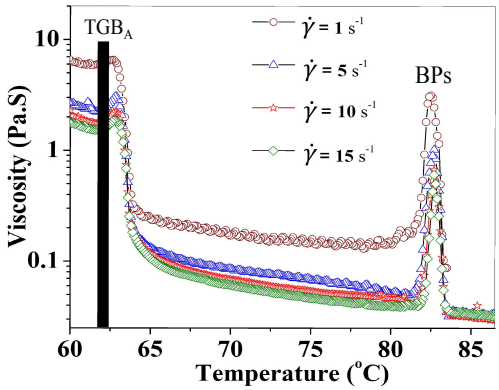

Figure 5. Temperature-dependent shear viscosity at different shear rates in a binary mixture of 80 wt % Cholesteryl Nonanoate (CN) and 20 wt % 4′-octyloxy-4-cyanobiphenyl (8OCB). The black bar shows the narrow temperature range of the induced TGB$_A$ phase. Measuring device: cone-plate with a plate diameter of 25 mm and a cone angle of 1°. Reproduced with permission from [12].

Figure 7a shows the shear rate-dependent shear stress of different phases of the mixture. At a low shear rate, where $\dot{\gamma} \to 0$, the shear stress tends to reach a constant value showing an apparent yield stress (σ_y). Figure 7b shows the variation of yield stress at different phases. In the N* phase, σ_y is negligibly small (10^{-2} Pa). In the TGB$_A$ phase, $\sigma_y \simeq 10$ Pa. Thus, the yield stress of TGB$_A$ is three orders of magnitude larger than that of the N* phase. However, the apparent yield stress of the TGB$_A$ phase of the studied mixture is much larger than that known for low molecular weight smectic liquid crystals [28,29].

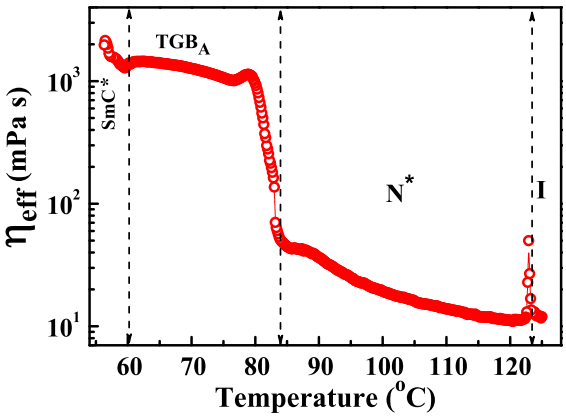

Figure 6. (Color online) Variation of effective shear viscosity (η_{eff}) as a function of temperature at a constant shear rate 100 s^{-1}. Measuring device: cone-plate with a plate diameter of 25 mm and a cone angle of 1°. Reproduced with permission from [25].

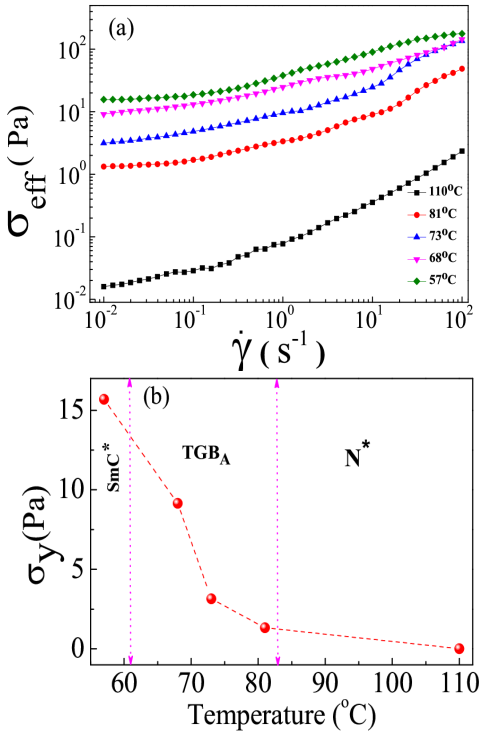

Figure 7. (Color online) (**a**) Shear rate-dependent effective shear stress (σ_{eff}) at different temperatures corresponding to different phases; (**b**) yield stress (σ_y) at different temperatures. Measuring device: cone-plate with a plate diameter of 25 mm and a cone angle of 1°. Reproduced with permission from [25].

The frequency-dependent shear modulus ($G^{'}$ and $G^{''}$) provides the dynamic response of the sample. Figure 8 shows some representative frequency dependence of storage ($G^{'}$) and loss moduli ($G^{''}$) in the N^* and TGB_A phases. The role of defects and disorder on the viscoelastic properties of randomly-oriented Type-I smectic liquid crystals has been studied by many authors [4,30–36]. In the reported systems, the defects were either stabilized by quenched disorder or by dispersing colloidal particles in the liquid crystals. The storage modulus ($G^{'}$) of such a system shows a power-law behavior:

$$G^{'}(\omega) = G_0 + \beta\omega^{\alpha} \quad (3)$$

where G_0 is the plateau modulus arising from the zero frequency shear modulus, ω is the angular frequency, β is a constant and α is an exponent. The TGB_A is composed of rotating SmA blocks separated by grain boundaries made of parallel screw dislocations. These defects are inbuilt into the structure, and hence, cannot disappear due to the action of shear. The contribution of defects and disorder to the rheological properties of the TGB_A is analyzed by the same model. α obtained from the fitting of $G^{'}(\omega)$ and $G^{''}(\omega)$ at different temperatures is shown in Figure 9. In the N^* phase, α obtained from the fitting of $G^{'}$ and $G^{''}$ is about two and one, respectively. The exponent α decreases in the TGB_A phase and is almost equal to $\alpha \simeq 0.5$. The solid-like behavior reflected by a plateau in $G^{'}$ in the terminal zone has been studied and characterized theoretically in other mesophases, such as carbonaceous mesophases [37]. The storage modulus of liquid crystalline systems with a defect network has been experimentally studied by Ramos et al. [38]. They showed that the contributions from the disoriented part of the sample and regions of the sample where the layers are parallel to the shear direction are given by $G^{'} \propto \omega^{1/2}$ and $G^{'} \propto \omega^{2}$ respectively. Similarly the loss modulus has a contribution both from the disorientated parts ($G^{''} \propto \omega^{1/2}$) of the sample and a Maxwell fluid type contribution ($G^{''} \propto \omega$). In the TGB_A phase, α obtained from the fitting of $G^{'}$ and $G^{''}$ is equal and given by $\alpha \simeq 0.5$. Hence, the storage and loss moduli have a major contribution from the disorientated layers of the TGB_A phase.

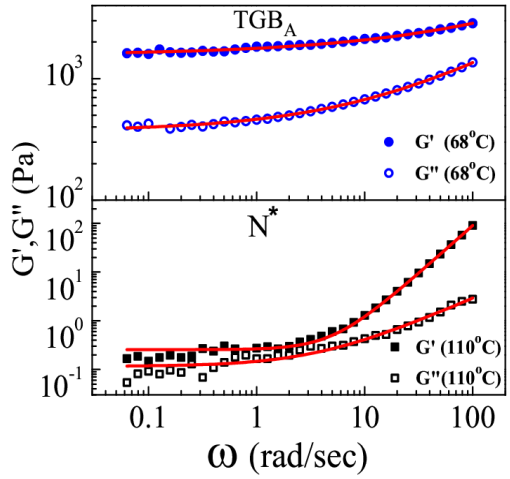

Figure 8. (Color online) Frequency dependence of storage $G^{'}$ (solid symbols) and loss $G^{''}$ (open symbols) moduli at two representative temperatures in the N^* and TGB_A phases. The solid lines are the best fits to Equation (3). Measuring device: cone-plate with a plate diameter of 25 mm, a cone angle of 1° and $\gamma = 1$. Reproduced with permission from [25].

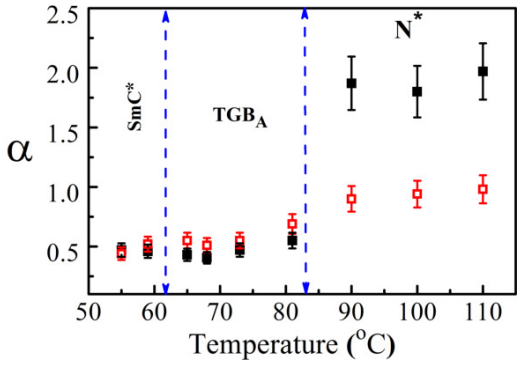

Figure 9. (Color online) The temperature variation of exponent α obtained by fitting the power-law equation (Equation (3)). The data corresponding to solid squares are obtained by fitting the storage modulus ($G^{'}$), and open squares are obtained by fitting the loss modulus ($G^{''}$). Reproduced with permission from [25].

According to the soft glass rheology model, the glass transition is characterized by the power-law exponent, i.e., $G^{'} \sim \omega^{x-1}$. In this model, "x" is an effective noise temperature that varies within $1 < x < 2$ and is related to the exponent α by $\alpha = x - 1$ [39]. The system approaches the glass transition if $x \to 1$, i.e., $\alpha \to 0$. In reference to Figure 9, across the N^* to TGB_A phase transition, x decreases from three to about 1.5, signifying that the rheological response of TGB_A is very close to many soft glassy materials.

The temperature variation of G_0 is directly related to the defects. The variation of G_0 with reduced temperature $\chi \equiv (T_{N^*\text{-}TGB_A} - T)/(T_{N^*\text{-}TGB_A})$ is shown in Figure 10. In the TGB_A phase, G_0 is more than three orders of magnitude larger than the N^* phase (Figure 10). In connection to the rubber elasticity, the elastic response of static defect network G_0 varies as $G_0 \approx \tau/d^2$, where τ is the line tension and d is a typical average spacing between defects [38]. The defect line tension τ can be expressed as $\tau = Bb^4/128\pi^3 r_c^2$, where B is the layer compression modulus, $b = md_0$ is the Burger vector of integer strength m and r_c is the defect core radius [40]. There are many smectic liquid crystals in which $B \sim \chi^{0.4}$ [41] and $r_c^{-2} \sim \psi^2 \sim \chi^{0.5}$, where ψ is the smectic order parameter [42]. Hence, the defect line tension (τ) varies as $\tau \sim \chi^{0.9}$. This implies that the elasticity of the static defect network varies as $G_0 \sim \chi^{\gamma}$ with $\gamma \approx 0.9$ [42]. Figure 10 shows the variation of G_0 with the least square fit parameter $\gamma = 1$. Assuming a medium value of Berger's vector of integer strength $m = 2$ [43], $B \approx 2 \times 10^6$ Pa [30,41] and using the relation $G_0 \approx \tau/d^2$, the calculated inter-defect spacing in the TGB_A phase is $d \approx 26$ nm. This calculated value is closely comparable with the experimentally-measured dislocation spacing in the TGB_A phase [7].

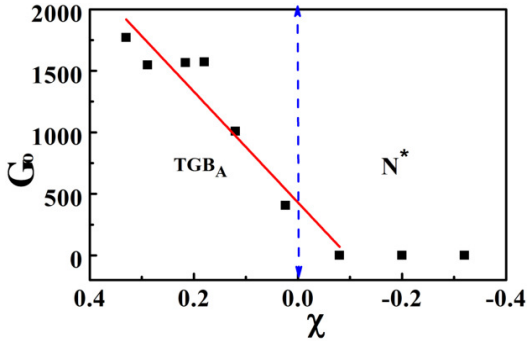

Figure 10. (Color online) Variation of G_0 with reduced temperature: $\chi \equiv (T_{N^*\text{-}TGB_A} - T)/(T_{N^*\text{-}TGB_A})$. The solid line shows the best fit to $G_0 \simeq \chi^{\gamma}$, with $\gamma = 1$. Reproduced with permission from [25].

4. Rheological Properties of Blue Phases

Recently, several theoretical predictions are made on the rheological properties of blue phases [20–22]. However, experimentally, it is much less explored due to its narrow range of temperature. The rheological properties of BPs with a narrow range of temperature in CN were first reported by Kleiman et al. [44]. It exhibits the following phase transitions: I 90.52 °C BP-I 91.00 °C BP-II 91.08 °C BP-III 91.22 °C N^*. It shows three blue phases, and the temperature ranges of BP-III, BP-II and BP-I are 14 mK, 8 mK and 48 mK, respectively. Figure 11 shows the storage modulus and viscosity as a function of temperature. They showed that BP-I and BP-II are viscoelastic solids and that BP-III has cholesteric-like order.

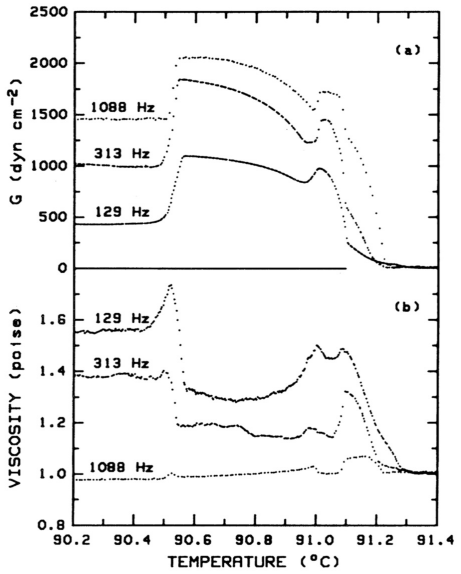

Figure 11. The elastic modulus and viscosity of CN at three different frequencies across the Isotropic (I)-N* transition showing three blue phases. Measuring device: torsional oscillators configured as cup viscometers with a cup diameter of 0.51 cm. Reproduced with permission from [44].

Very recently, Rasmita et al. made detailed experimental studies on the rheology of BPs by taking a mixture of four fluorinated compounds and a highly chiral dopant [26,45]. It exhibits the following phase transitions: I 46.4 °C, BP-II 41.4 °C BP-I 36.6 °C N*. The temperature ranges of BP-I and BP-II are 4.8 °C and 5 °C, respectively, and much larger than the CN compound. The temperature-dependent shear stress at a fixed shear rate of the mixture is shown in Figure 12. Distinct changes of stress (τ) across the phase transitions are clearly observed. A small kink in the stress-curve marks the BP-II to BP-I phase transition. The shear stress of BP-I is larger than that of BP-II and N* phase. This is consistent with the previous report, i.e., the elasticity of the BP-I is greater than that of BP-II.

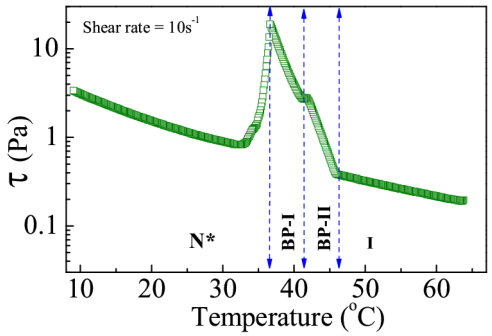

Figure 12. (Color online) Temperature-dependent shear stress at a constant shear rate (10 s^{-1}). Three different phase transitions are marked by dotted vertical lines. Measuring device: cone-plate with a plate diameter of 25 mm and a cone angle of 1°. Reproduced with permission from [26].

Simultaneous optical rheomicroscopy measurements reveal the change in the textures across the phase transitions. For example, Grandjean–Cano lines are observed in the BP-II phase, and they are aligned perpendicular to the shear direction (Figure 13a). The increase of shear stress as compared to the isotropic phase is due to the motion of the Grandjean–Cano lines. With decreasing temperature, some filamentary structures appear in the BP-I phase. This corresponds to the increase in shear stress in the BP-I phase as compared to the BP-II phase (Figure 13b). These filamentary structures are continuously broken and reconnected under steady shear. The N* phase (Figure 13c,d) shows

a typical texture of oily-streak defects. Dupuis et al. have studied the rheology of cholesteric blue phases by computer simulation [22]. It was predicted that the shear forces can bend, twist and unlock the disclination lines. Under low shear, the defect network opposes the flow; hence, the apparent shear viscosity and shear stress become large. However, under high shear, they show shear thinning behavior signifying the disruption of the defect network.

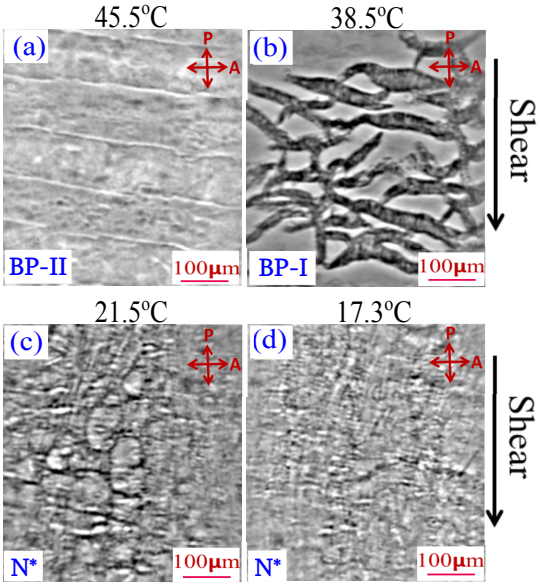

Figure 13. Optical rheomicroscopy images taken during the measurement of temperature-dependent shear stress at a constant shear rate of 10 s^{-1} in three different phases. The direction of shear is shown by an arrow. P and A indicate Polarizer and Analyzer. Measuring device: rheomicroscopy setup with a parallel plate of diameter 43 mm. The gap between the two parallel glass plates is 0.075 mm. Reproduced with permission from [26].

The flow behaviors of the BP-II, BP-I and N^* phases are shown in Figure 14. The N^* phase exhibits a typical shear thinning behavior. The yield stresses of BP-II and BP-I are about one order of magnitude larger as compared to the N^* phase. BP-I and BP-II both exhibits multiple shear thinning behavior at a higher shear rate range. The shear stress of BP-II shows three distinct regimes, i.e., BP-II(1): $\dot{\gamma}$ = 0.01–0.3 s^{-1}; BP-II(2): $\dot{\gamma}$ = 0.3–2 s^{-1} and BP-II(3): $\dot{\gamma}$ = 2–1000 s^{-1}. Figure 14b shows a power-law fit; $\tau = a\dot{\gamma}^{\alpha}$, which describes the data to a very good approximation. The fit parameters are: a = 0.87 and α = 0.33 in BP-II(1); a = 0.42 and α = 0.35 in BP-II(2); a = 0.12 and α = 0.87 in BP-II(3).

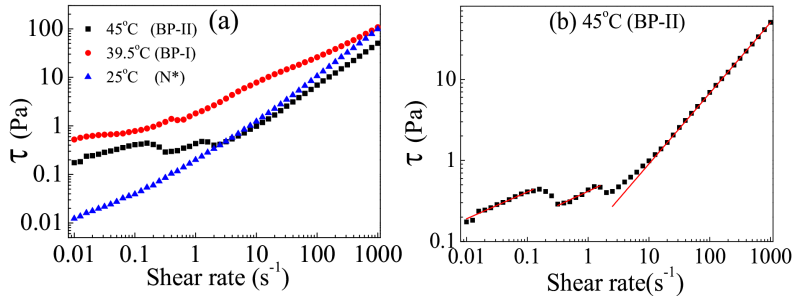

Figure 14. (Color online) (**a**) Shear rate-dependent shear stress at three different temperatures representing the BP-II, BP-I and N^* phases; (**b**) red lines are best fits to the power-law: $\tau = a\dot{\gamma}^{\alpha}$ in the BP-I phase. Measuring device: cone-plate with a plate diameter of 25 mm and a cone angle 1°. Reproduced with permission from [26].

Rheomicroscopy images at some representative shear rates are shown in Figure 15. In a low shear rate regime (0.01–0.3 s^{-1}), in the BP-II phase, the Grandjean–Cano lines flow parallel to the shear direction (downward green arrows in BP-II). In the intermediate shear rate region (0.3–2 s^{-1}), these Grandjean–Cano lines are broken, and at a higher shear rate-range (2–1000 s^{-1}), the system shows a flow-aligned nematic-like state. The BP-I also shows multiple shear thinning regimes, but they are not clearly separable like BP-II. However, it is clear that multiple shear thinning is due to the breaking of texture at different shear rates as shown in Figure 15 (see BP-I). The N^* phase shows uniform shear thinning behavior, and there are no notable changes observed in the textures up to the shear rate of 10 s^{-1}. Above this shear rate, probably the helix uncoils, and the sample flows like nematic, causing a decrease in the viscosity. Both BP-II and BP-I also exhibit the flow-induced nematic texture at a shear rate much higher than 200 s^{-1}.

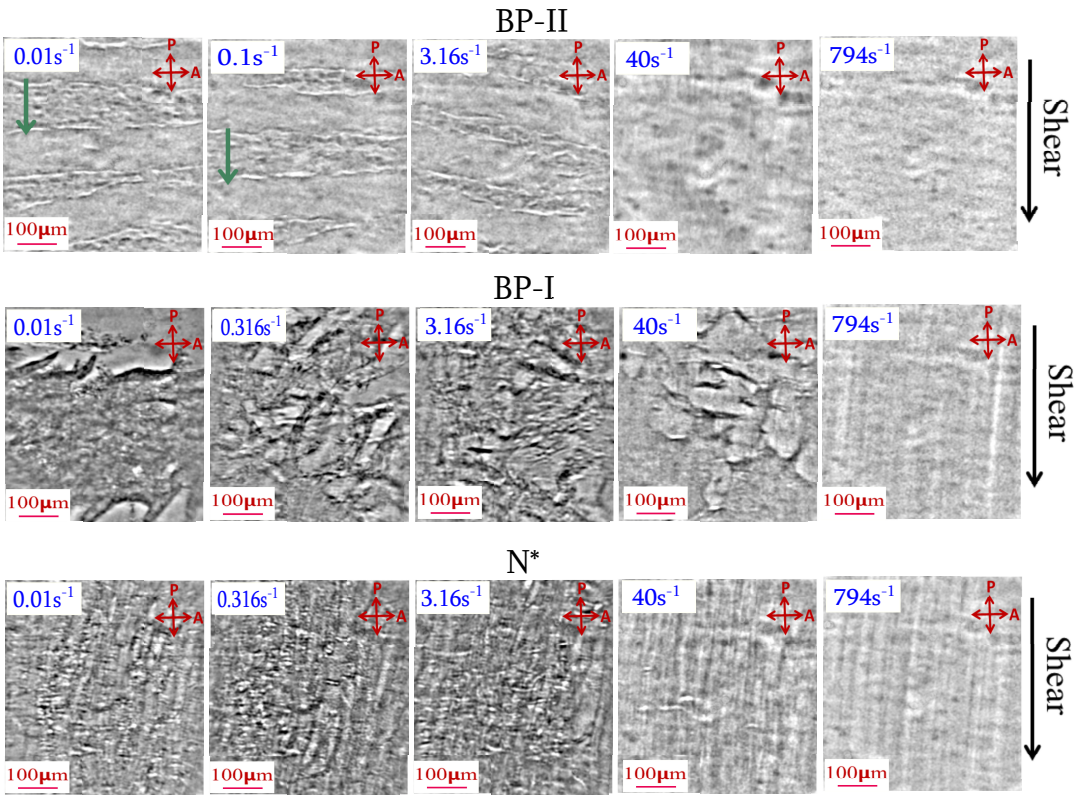

Figure 15. Rheomicroscopy images taken between two crossed polarizers during the measurement of the shear rate-dependent shear stress in three different phases. The direction of shear is shown by an arrow on the right-hand side. The downward green arrows in BP-II show the motion of the Grandjean–Cano lines. Measuring device: rheomicroscopy setup with the parallel plate of a diameter of 43 mm. The gap between two parallel glass plates is 0.075 mm. Reproduced with permission from [26].

Recently, Henrich et al. studied the rheology of cubic blue phases by computer simulation [20,21,23]. They have identified various flow regimes with increasing shear rate in both BP-I and BP-II. The typical flow curve in both phases is shown in Figure 16. Experimental results of Figure 14 qualitatively agree with the predictions of the simulation except that shear rate ranges are different.

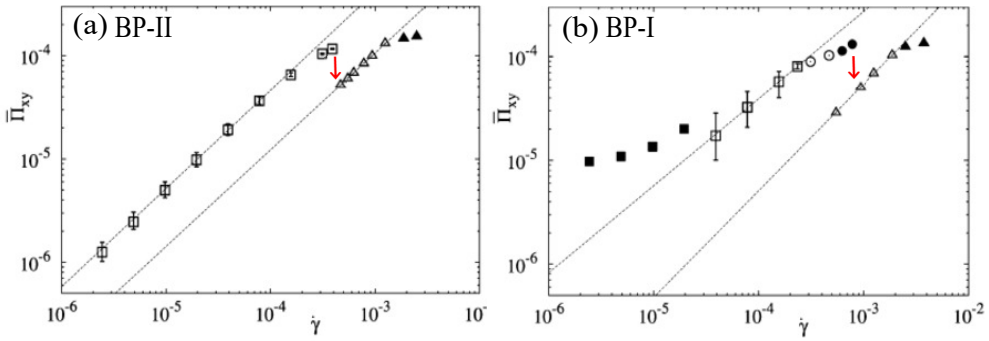

Figure 16. Flow curve of shear rate-dependent shear stress showing various flow regimes of (**a**) BP-II and (**b**) BP-I. Above a critical shear rate, the network breaks up into the Grandjean texture (open triangles) or a flow-aligned nematic state at even higher shear rates (solid triangles). The red arrows indicate a fall in the shear stress values. In the simulation, a simple shear flow was imposed by means of the Lees–Edwards boundary conditions with the top (bottom) part of the system flowing in the positive (negative) x-direction and the velocity gradient along the y-direction. The shear rates were varied over more than three orders of magnitude. Reproduced with permission from the [21].

The deformation behavior of blue phases is further studied by the amplitude sweep. The results of amplitude sweep, i.e., the strain-dependent storage ($G^{'}$) and the loss ($G^{''}$) moduli at different temperatures representing different phases (BP-II, BP-I and N*), are shown in Figure 17. The N* phase shows a typical fluid-like behavior. The shear moduli of both the blue phases (BP-II and BP-I) are higher than that of the N* phase. The storage modulus ($G^{'}$) of BP-I is about five-times larger than that of BP-II. The Linear Visco-Elastic (LVE) ranges of both BP-II and BP-I are almost equal, i.e., γ_{LVE} = 4%. The strain-induced fluidization (the crossover of $G^{'}$ and $G^{''}$), or the critical strain amplitude denoted by γ_c, is 16% in the case of BP-I. However, in BP-II, it occurs at a slightly higher strain value (γ_c = 20%) than that of BP-I. It was interpreted that in BP-II, the defect lines intersect with each other, which needs a larger strain amplitude to break.

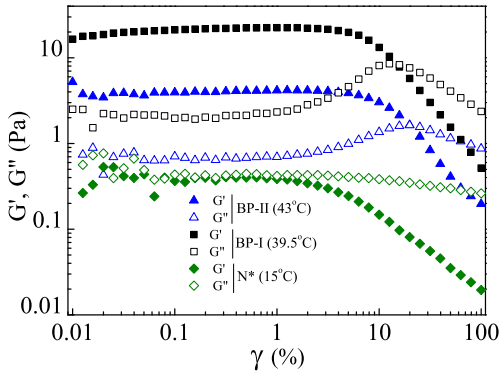

Figure 17. (Color online) The strain dependence of the storage ($G^{'}$) and the loss ($G^{''}$) moduli of the sample at three different temperatures at ω = 1 rad s^{-1}. Measuring device: cone-plate with a plate diameter of 25 mm and a cone angle of 1°. Reproduced with permission from [26].

The dynamics of the defect networks are investigated by a step-strain measurement. Figure 18a shows the shear stress response with time under the applied step strain. The applied strain is changed with time stepwise from 0.3–30% and then again back to 0.3%. Therefore, there are three regions with two steps in which 0.3% is within the LVE range and 30% is above the LVE range. The duration of each step is 600 s. The N* phase shows a typical stress response under applied step strain in all the regions, as expected. Both BP-II and BP-I exhibit different responses in Region-II and Region-III than the cholesteric phase. In Region-II of BP-II, a gradual decrease of shear stress with time is

observed. It could be due to the breaking of defect nodes under high strain followed by a continuous flow-aligned state. In Region-II of BP-I, a constant shear stress response is observed. BP-I shows sinusoidal oscillations of shear stress with time in Region-III that decays with time. Figure 18b shows the periodic modulation of stress with time in Region-III of BP-I. Stress oscillation after cessation of shear in chiral liquid crystals has been simulated and characterized for cholesteric liquid crystals [46]. The oscillation in shear stress of BP-I is attributed to the lattice distortion, i.e., displacement of defects from the equilibrium positions. The equilibrium structure tends to be restored upon removal of the strain, which gives rise to periodic stress oscillation, which decays with time [25]. Hence, the step strain experiment reveals the different dynamical behavior of BP-I and BP-II due to their distinct defect structures.

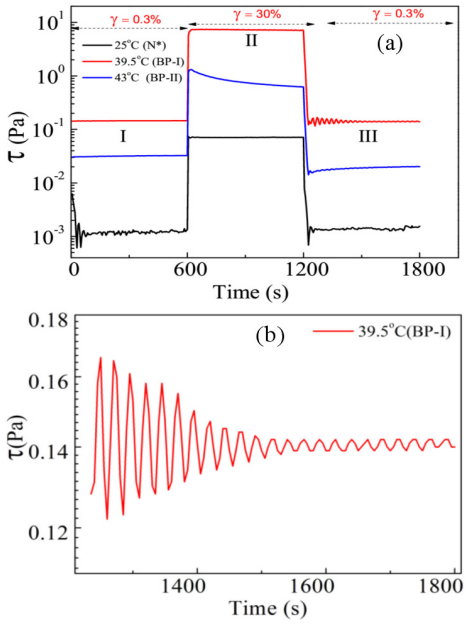

Figure 18. (Color online) (**a**) Time-dependent shear stress at three different temperatures for ω = 1 rad/sec; (**b**) enlarged area of BP-I in Region-III (see (a)) showing the periodic stress oscillation. Measuring device: cone-plate with a plate diameter of 25 mm and a cone angle of 1°. Reproduced with permission from [26].

5. Conclusions

Rheological properties of two liquid crystalline intermediate phases in highly chiral liquid crystals namely TGB_A and BPs are presented. Topological defects are inherent to both phases and contribute to the rheological properties. The analysis of the complex shear modulus shows that the elasticity of the TGB_A phase is due to the contribution of inbuilt structural defects. The TGB_A liquid crystals are a defect-mediated soft solid whose dynamics is similar to soft glassy materials. Simple calculations based on the theory of rubber elasticity provide the inter-dislocation distance. Both BP-II and BP-I show several flow regimes with characteristic microstructures. The experimental results are qualitatively in agreement with some recent results of computer simulation. Both blue phases exhibit a solid-like behavior, while the cholesteric phase shows a gel-like behavior. The sinusoidal stress oscillations in BP-I after the removal of strain are connected to the dynamic response of the distinct defect structures. The critical strain amplitude for strain-induced fluidization, i.e., γ_c of BP-II is larger than that of BP-I, and it is attributed to the defect structure; in particular, the breaking of defect nodes in BP-II requires larger strain than BP-I. Finally, it may be mentioned that there are several predictions on the dynamic behavior of defects in the blue phases from the computer simulations, and to validate them, more experiments are required.

Acknowledgments: We gratefully acknowledge the support from Depart of Science and Technology (Project Ref.: DST/SJF/PSA-02/2014-2015).

Conflicts of Interest: The authors declare no conflict of interest.

References

1. De Gennes, P.G.; Prost, J. *The Physics of Liquid Crystals*; Clarendon Press: Wotton-under-Edge, UK, 1993.
2. Chandrasekhar, S. *Liquid Crystals*; Cambridge University Press: Cambridge, UK, 1992.
3. Chaikin, P.M.; Lubensky, T.C. *Principle of Condensed Matter Physics*; Cambridge University Press: Cambridge, UK, 1998.
4. Zapotocky, M.; Ramos, L.; Poulin, P.; Lubensky, T.C.; Weitz, D.A. Particle-stabilized defect gel in cholesteric liquid crystals. *Science* **1999**, *283*, 209–212.
5. Renn, S.R.; Lubensky, T.C. Abrikosov dislocation lattice in a model of the cholesteric-to-smectic-A transition. *Phys. Rev. A* **1988**, *38*, 2132.
6. Goodby, J.W.; Waugh, M.A.; Stein, S.M.; Chin, E.; Pindak, R.; Patel, J.S. Characterization of a new helical smectic liquid crystal. *Nature* **1989**, *337*, 449–452.
7. Navailles, L.; Pansu, B.; Gorre-Talini, L.; Nguyen, H.T. Structural study of a commensurate TGB_A phase and of a presumed chiral line liquid phase. *Phys. Rev. Lett.* **1998**, *81*, 4168.
8. Nguyen, H.T.; Bouchta, A.; Navailles, L.; Barois, P.; Isaert, N.; Twieg, R.J.; Maaroufi, A.; Destrade, C. TGB_A and TGB_C phases in some chiral tolan derivatives. *J. Phys. II France* **1992**, *2*, 1889–1906.
9. Galerne, Y. The commensurate and incommensurate $TGBC^*$ liquid crystal phases. *Eur. Phys. J. E* **2000**, *3*, 355–368.
10. Pramod, P.A.; Pratibha, R.; Madhusudana, N.V. A three-dimensionally modulated structure in a chiral smectic-C liquid crystal. *Curr. Sci.* **1997**, *73*, 761–765.
11. Dhara, S.; Pratibha, R.; Madhusudana, N.V. Some experimental investigations on Type II Chiral Liquid Crystals. *Ferroelectrics* **2002**, *277*, 13–23.
12. Rajeswari, M.; Ananthaiah, J.; Dabrowski, R.; Sastry, V.S.S.; Dhara, S.; Sadashiva, B.K. Rheological properties of a chiral liquid crystal exhibiting Type-II character. *Mol. Cryst. Liq. Cryst.* **2011**, *547*, 39–45.
13. Grebel, H.; Hornreich, R.M.; Shtrikman, S. Landau theory of cholesteric blue phases: The role of higher harmonics. *Phys. Rev. A* **1984**, *30*, 3264.
14. Wright, D.C.; Mermin, N.D. Crystalline liquids: the blue phases. *Rev. Mod. Phys.* **1989**, *61*, 385.
15. Kikuchi, H.; Yokota, M.; Hisakado, Y.; Yang, H.; Kajiyama, T. Polymer-stabilized liquid crystal blue phases. *Nat. Mater.* **2002**, *1*, 64–68.
16. Chen, K.M.; Gauza, S.; Xianyu, H.Q.; Wu, S.T. Submillisecond gray-level response time of a polymer-stabilized blue-phase liquid crystal. *J. Disp. Technol.* **2010**, *6*, 49–51.
17. Rao, L.; Ge, Z.; Wu, S.T.; Lee, S.H. Low voltage blue-phase liquid crystal displays. *Appl. Phys. Lett.* **2009**, *95*, 231101.
18. Kim, M.S.; Kim, M.; Jung, J.H.; Ha, K.S.; Yoon, S.; Song, E.G.; Srivastava, A.K.; Choi, S.W.; Lee, G.D.; Lee, S.H. Blue phases liquid crystal cell driven by strong in-plane electric field. *SID Int. Symp. Dig. Tech. Pap.* **2009**, *40*, 1615–1618.
19. Rahman, M.D.A.; Said, S.M.; Balamurugan, S. Blue phase liquid crystal: strategies for phase stabilization and device development. *Sci. Technol. Adv. Mater.* **2015**, *16*, 033501.
20. Henrich, O.; Stratford, K.; Marenduzzo, D.; Coveney, P.V.; Cates, M.E. Confined cubic blue phases under shear. *J. Phys. Condens. Matter.* **2012**, *24*, 284127.
21. Henrich, O.; Stratford, K.; Coveney, P.V.; Cates, M.E.; Marenduzzo, D. Rheology of cubic blue phases. *Soft Matter.* **2013**, *9*, 10243–10256.
22. Dupuis, A.; Marenduzzo, D.; Orlandini, E.; Yeomans, J.M. Rheology of Cholesteric Blue Phases. *Phys. Rev. Lett.* **2005**, *95*, 097801.
23. Henrich, O.; Stratford, K.; Marenduzzo, D.; Cates, M.E. Ordering dynamics of blue phases entails kinetic stabilization of amorphous networks. *Proc. Natl. Acad. Sci. USA* **2010**, *107*, 13212–13215.
24. Henrich, O.; Marenduzzo, D.; Stratford, K.; Cates, M.E. Thermodynamics of blue phases in electric fields. *Phys. Rev. E* **2010**, *81*, 031706.

25. Sahoo, R.; Ananthaiah, J.; Dabrowski, R.; Dhara, S. Rheology of twist-grain-boundary-A liquid crystals. *Phys. Rev. E* **2014**, *90*, 012506.
26. Sahoo, R.; Chojnowska, O.; Dabrowski, R.; Dhara, S. Experimental studies on the rheology of cubic blue phases. *Soft Matter.* **2016**, *12*, 1324–1329.
27. Asnacios, S.; Meyer, C.; Nastishin, Y.A.; Kleman, M.; Malthete, J. Rheological properties of chiral liquid crystals possessing a cholesteric-smectic A transition. *Liq. Cryst.* **2004**, *31*, 593–599.
28. Chapoy, L.L.; Duke, R.W. Some anomalous rheological responses of thermotropic liquid crystals. *Rheol. Acta* **1979**, *18*, 537–544.
29. Paasch, S.; Schambil, F.; Schwuger, M.J. Rheological properties of lamellar lyotropic liquid crystals. *Langmuir* **1989**, *5*, 1344–1346.
30. Bandyopadhyay, R.; Liang, D.; Colby, R.H.; Harden, J.L.; Leheny, R.L. Enhanced elasticity and soft glassy rheology of a smectic in a random porous environment. *Phys. Rev. Lett.* **2005**, *94*, 107801.
31. Basappa, G.; Suneel Kumaran, V.; Nott, P.R.; Ramaswamy, S.; Naik, V.M.; Rout, D. Structure and rheology of the defect-gel states of pure and particle-dispersed lyotropic lamellar phases. *Eur. Phys. J. B* **1999**, *12*, 269–276.
32. Fujii, S.; Komura, S.; Ishii, Y.; Lu, C.Y.D. Elasticity of smectic liquid crystals with focal conic domains. *J. Phys. Condens. Matter* **2011**, *23*, 235105.
33. Roth, M.; Acunzi, M.D.; Vollmer, D.; Auernhammer, G.K. Viscoelastic rheology of colloid-liquid crystal composites. *J. Chem. Phys.* **2010**, *132*, 124702.
34. Meyer, C.; Asnacios, S.; Bourgaux, C.; Kleman, M. Rheology of lyotropic and thermotropic lamellar phases. *Rheol. Acta* **2000**, *39*, 223–233.
35. Kawasaki, K.; Onuki, A. Dynamics and rheology of diblock copolymers quenched into microphase-separated states. *Phys. Rev. A* **1990**, *42*, 3664(R).
36. Larson, R.G.; Winey, K.I.; Patel, S.S.; Watanabe, H.; Bruinsma, R. The rheology of layered liquids: lamellar block copolymers and smectic liquid crystals. *Rheol. Acta* **1993**, *32*, 245–253.
37. Lima, L.R.; Rey, A.D. Linear viscoelasticity of textured carbonaceous mesophases. *J. Braz. Chem. Soc.* **2006**, *1109*, 17.
38. Ramos, L.; Zapotocky, M.; Lubensky, T.C.; Weitz, D.A. Rheology of defect networks in cholesteric liquid crystals. *Phys. Rev. E* **2002**, *66*, 031711.
39. Sollich, P.; Lequeux, F.; Hebraud, P.; Cates, M.E. Rheology of soft glassy materials. *Phys. Rev. Lett.* **1997**, *78*, 2020.
40. Kleman, M. Defects in liquid crystals. *Rep. Prog. Phys.* **1989**, *52*, 555.
41. Benzekri, M.; Marcerou, J.P.; Nguyen, H.T.; Rouillon, J.C. Critical behavior of the layer compressional elastic constant B at the smectic-A-nematic phase transition. *Phys. Rev. B* **1990**, *41*, 9032.
42. Leheny, R.L.; Park, S.; Birgeneau, R.J.; Gallani, J.L.; Garland, C.W.; Iannacchione, G.S. Smectic ordering in liquid-crystal-aerosil dispersions. I.X-ray scattering. *Phys. Rev. E* **2003**, *67*, 011708.
43. Kamien, R.D.; Lubensky, T.C. Minimal surfaces, screw dislocations and twist grain boundaries. *Phys. Rev. Lett.* **1999**, *82*, 2892.
44. Kleiman, R.N.; Bishop, D.J.; Pindak, R.; Taborek, P. Shear modulus and specific heat of the liquid-crystal blue phases. *Phys. Rev. Lett.* **1984**, *53*, 2137.
45. Chojnowska, O.; Dabrowski, R.; Yan, J.; Chen, Y.; Wu, S.T. Electro-optical properties of photochemically stable polymer-stabilized blue-phase material. *J. Appl. Phys.* **2014**, *116*, 213505.
46. Rey, A.D. Structural transformations and viscoelastic response of sheared fingerprint cholesteric textures. *J. Non-Newton. Fluid Mech.* **1996**, *64*, 207–227.